Origin of second harmonic generation in gold plasmonic nanostructures

Sanro Mathew, Maeliss Ethis de Corny, Nicolas Chauvet, Laureen Moreaud, Guillaume Laurent, Serge Huant, Erik Dujardin, Gilles Nogues, Guillaume Bachelier

Origin of second harmonic generation in gold plasmonic nanostructures

S.Mathew[a], M.Ethis de Corny[a], N.Chauvet[a], L.Moreaud[b], G.Laurent[a], S.Huant[a], E.Dujardin[b,c], G.Nogues[a], and G.Bachelier[a]

[a]Institut Néel - CNRS, Université Grenoble Alpes, Grenoble, France
[b]CEMES - CNRS, Toulouse, France
[c]Laboratoire Interdisciplinaire Carnot de Bourgogne CNRS, Université Bourgogne Franche-Comté, Dijon, France

ABSTRACT

The second harmonic generation in gold nanoprisms is investigated numerically and experimentally. Comparing the experimentally obtained cartographic SHG maps with numerically simulated maps, we are able to discriminate between the different nonlinear source contributions as well as demonstrate the response that dominates in these nanostructures. Precisely, we show that the parallel surface current source dominates in these nanoprisms which has been a largely discarded source in the literature.

Keywords: Plasmonics, Nonlinear optics, Second-harmonic generation, Gold, Nanoprisms

1. INTRODUCTION

Nonlinear optical processes has been the subject of research for many decades owing to an interest in the pursuit of furthering the fundamental science as well as for its applications. In this context, second-order processes including second harmonic generation (SHG), difference frequency generation (DFG), sum frequency generation (SFG) and spontaneous parametric down conversion (SPDC) has been well studied in bulk media and utilized for frequency conversion as well as for entangled photon pair generation.[1,2] More recently, the advancement in nanofabrication techniques spurred by the growing demand for down scaling components to nanoscale size has led to a renewed interest in the research of nonlinear optics at the nanoscale. Owing to the ability of plasmonic metal nanostructures to confine and enhance electromagnetic field at the sub-wavelength scale, generation of nonlinearity, in particular SHG, from metal nanostructures has therefore been of significant interest.[3]

SHG is a process in which an incident wave at frequency ω is converted to an outgoing wave at 2ω. SHG is sensitive to material symmetry. It is forbidden in centrosymmetric materials within the electric dipole approximation.[1] Hence, the nonlinearity arises through different mechanisms and its description in metal nanostructures which are centrosymmetric has been the subject of numerous investigations. Briefly, these mechanisms correspond to symmetry breaking at the surface and higher order effects from multipoles within the bulk (magnetic dipole and electric quadrupole).[4,5] The separation of the effects from the different mechanisms has been addressed through several investigations. In the case of thin gold film, surface effects (arising from the normal component of surface polarization) is found to be the dominant contribution to the SHG response,[6] while, in the case of split ring resonators, bulk contribution is found to be dominant.[8] Regardless, in general it is widely believed that the contribution from normal surface component always dominate the nonlinear response as was concluded in a recent theoretical work.[9]

In this report, we compare experimental and simulated far-field SHG intensity distribution obtained under tightly focused laser beam excitation, and report that the dominant nonlinear contribution in gold nanoprisms arises from the parallel surface component which was considered to play a less significant role in the SHG process.

2. THEORETICAL FRAMEWORK

Due to the breaking of the inversion symmetry of centrosymmetric materials as in the case of metal interfaces, the conduction electrons experience an asymmetric potential that leads to second order nonlinearity in the induced currents.[4] Thus, for any isotropic material with an inversion symmetry, the second harmonic (SH) surface polarization can be expressed through three components of the susceptibility tensor as:[10]

$$\begin{aligned}\vec{P}_{surface}(r,2\omega) &= \epsilon_0\chi_{\perp\perp\perp}E_\perp(r,\omega)E_\perp(r,\omega)\mathbf{n}\\ &+ \epsilon_0\chi_{\parallel\parallel\perp}E_\parallel(r,\omega)E_\perp(r,\omega)\mathbf{k}\\ &+ \epsilon_0\chi_{\perp\parallel\parallel}E_\parallel(r,\omega)E_\parallel(r,\omega)\mathbf{n},\end{aligned} \tag{1}$$

where $\perp$ and $\parallel$ represents components perpendicular and parallel to the surface and $\mathbf{n}$ is the unit vector normal to the surface at point $\mathbf{r}$ while $\mathbf{k}$ being the unit vector parallel to the surface. For instance, $\chi_{\perp\parallel\parallel}$ denotes surface polarization perpendicular to the surface generated by components of electric field parallel to the surface. Although the susceptibility tensor is expressed through three components, the existing models of electron dynamics at the surface based on hydrodynamic model predicts $\chi_{\perp\parallel\parallel}$ to be vanishing.[10] Hence, the surface polarization reduces to:

$$\begin{aligned}\vec{P}_{surface}(r,2\omega) &= \epsilon_0\chi_{\perp\perp\perp}E_\perp(r,\omega)E_\perp(r,\omega)\mathbf{n}\\ &+ \epsilon_0\chi_{\parallel\parallel\perp}E_\parallel(r,\omega)E_\perp(r,\omega)\mathbf{k},\end{aligned} \tag{2}$$

Additionally, SH sources arising from the bulk due to higher order effects such as electric quadrupole in the case of isotropic and centrosymmetric material is expressed as:[6]

$$\begin{aligned}\vec{P}_{bulk}(r,2\omega) &= \beta\vec{E}(r,\omega)[\vec{\nabla}\cdot\vec{E}(r,\omega)]\\ &+ \gamma_{bulk}\vec{\nabla}[\vec{E}(r,\omega)\cdot\vec{E}(r,\omega)]\\ &+ \delta'[\vec{E}(r,\omega)\cdot\vec{\nabla}]\vec{E}(r,\omega),\end{aligned} \tag{3}$$

Within the bulk, the first term of Eq.3 is vanishing whereas the third term corresponding to δ' has a nonlinear susceptibility that is an order of magnitude smaller than the second term in the case of single beam SHG.[11] Hence, the bulk polarization can be reduced to:

$$\vec{P}_{bulk}(r,2\omega) = \gamma_{bulk}\vec{\nabla}[\vec{E}(r,\omega)\cdot\vec{E}(r,\omega)], \tag{4}$$

The bulk contribution expressed above is often known as non-local bulk because the gradient represents the spatial variation of square of the electric field. The nonlinear susceptibilities in the surface polarization and the material parameter β in the non-local bulk are expressed using Rudnick and Stern parameters as:[4 12]

$$\begin{aligned}\chi_{\perp\perp\perp} &= -\frac{a}{4}[\epsilon_r(\omega)-1]\frac{e\epsilon_0}{m\omega^2},\\ \chi_{\parallel\parallel\perp} &= -\frac{b}{2}[\epsilon_r(\omega)-1]\frac{e\epsilon_0}{m\omega^2},\\ \gamma_{bulk} &= -\frac{d}{8}[\epsilon_r(\omega)-1]\frac{e\epsilon_0}{m\omega^2},\end{aligned} \tag{5}$$

where $\epsilon_r(\omega)$ is the dielectric function of the material at frequency ω while e and m corresponds to electron charge and mass. The a, b and d are the non-dimensional Rudnick and Stern parameters included to weigh the relative contributions from the different nonlinear sources. Following the work of Bachelier et al., the values of these parameters are taken to be a=0.56-0.25i, d=1 and b=-0.1.[10]

As these sources are weighed with different parameters, their separability allows us to evaluate their independent contributions and to simulate their intensity distribution to identify their role in SHG. To this end, it was shown that non-local bulk polarization can be reformulated into an effective surface contribution as:[12]

$$\begin{aligned}\vec{P}_{eff,\perp}(r,2\omega) &= [\chi_{\perp\perp\perp}-\chi_{\perp\parallel\parallel}]\vec{E}_\perp(r,\omega)\vec{E}_\perp(r,\omega)\\ &+ [\chi_{\perp\parallel\parallel}+\frac{\gamma_b}{\epsilon(2\omega)}]\vec{E}(r,\omega)\vec{E}(r,\omega),\end{aligned} \tag{6}$$

Conventionally, the polarization sheet is placed outside and consequently the nonlinear currents are evaluated outside, while, the fundamental fields are evaluated inside the material. As $\chi_{\perp\parallel\parallel}$ is vanishing, the effective polarization can then be written as:

$$\begin{aligned}\vec{P}_{eff,\perp}(r,2\omega) &= \chi_{\perp\perp\perp}\vec{E}_{\perp}(r,\omega)\vec{E}_{\perp}(r,\omega) \\ &+ \frac{\gamma_b}{\epsilon(2\omega)}\vec{E}(r,\omega)\vec{E}(r,\omega),\end{aligned} \tag{7}$$

As it is evident in this expression, the nonlocal bulk contribution and surface contributions can thus be separated and this allows us to assign the leading contribution to SHG.

3. FINITE ELEMENT SIMULATIONS

The separability of the nonlinear contributions thus allows us to simulate them independently to obtain their SHG response maps. The simulations were performed combining analytical methods (via MATLAB) and finite element method (via COMSOL). The simulation was designed to take into account the optical experimental setup that was developed. In a first step, the background field at the fundamental frequency (ω) is evaluated analytically by considering its transmission through a microscope objective, immersion oil and refraction through a glass substrate hosting the nanostructures. Thereafter, using the scattered field formulation, Maxwell's equations are solved to obtain the total field at the fundamental frequency. Then, the nonlinear source currents are computed taking into account the nonlinear susceptibilities given above in the expressions 5-7. In the next step, Maxwell's equations are again solved using these nonlinear sources to compute the harmonic field (2ω) and then the response currents generated by the harmonic field is computed which thereby gives the total current generated in the nanostructure. Finally, the field radiated by the nonlinear currents into the far field is evaluated analytically by taking into account its transmission back through the substrate and the objective lens onto a detector to obtain the SHG response.

4. NANOFABRICATION AND EXPERIMENTAL PROTOCOL

The protocol used for the fabrication of nanoprisms involves standard E-beam lithography and nanofabrication procedures as well as chemical synthesis for crystalline prisms. The samples were fabricated on a $170\mu m$ glass substrate (Zeiss 1.5 coverslip). In a first step, the substrates were cleaned in Nitric acid bath for one minute followed by rinsing using deionized water. Thereafter, substrates immersed in acetone were put in an ultrasound bath for three minutes. In a final step, the substrates were then subjected to an oxygen plasma cleaning for five minutes. Once the cleaning was performed, the substrates were then spin coated with 3% PMMA resist at 4000 rpm/s for 30 seconds and hard-baked for five minutes at 180°C. To dissipate charges from the E-beam exposure, the substrates were then spin coated with an electronic conductive resist Elektra92 (ARPC 5090) at 3500 rpm/s for 60 seconds followed by a soft bake at 90°C for two minutes. Following the E-beam exposure, the conductive resist was removed by rinsing in deionized water for one minute. Thereafter, the exposed resist is developed in Methyl Isobutyl Ketone and Isopropanol (MIBK/IPA) mixture composed in the ratio 1:3 for one minute which is followed by a rapid rinse in isopropanol in a first bath and then two minutes in a second bath of isopropanol as well. In the next step, Gold is deposited using electron gun evaporation of the desired thickness which is finally followed by a lift-off of the unexposed resist, in which, the substrate is immersed in N-methyl-2-pyrrolidone at 80°C for one hour and then rinsed with acetone and isopropanol. On the other hand, chemically synthesized prisms were prepared by using polyvinylpyrrolidone (PVP) and potassium iodide (KI) to reduce gold salt at room temperature. The desired shape, in our case, prisms, are obtained by controlling the pH of the solution. Additionally the dimension of the structures is controlled by the length of solution resting time. Finally, the prisms deposited at the bottom of solution are collected and dispersed on to a substrate.

The characterization of the nanoprisms were performed on an optical setup designed in a way to reach single particle sensitivity i.e to be able to perform single particle measurements. The signal from nanoprisms were collected through an oil immersion objective in reflection mode. For this purpose, a 100x objective of numerical aperture 1.3 is used, thus, providing diffraction limit resolution of 340nm and 170nm corresponding to the fundamental and harmonic wavelengths. The objective and the sample is mounted on a piezo electric

stage for longitudinal and lateral scanning. The chromatic aberration induced by the objective is corrected by using motorized telescopes to overlap the focal planes at the excitation and the collection wavelength. In addition to the motorized telescopes and piezoelectric stage control, a tracking algorithm is developed to automatically optimize the signal acquisition. A pulsed femtosecond Ti:Sapphire oscillator was used as the laser source which delivers 100fs pulses at a repetition rate of 80MHz. The average input power was set at $200\mu W$ to avoid excessive damage on the nanoprisms of interest.

5. RESULTS AND DISCUSSION

In order to probe the origin of nonlinear response from nanoprism antennas, we compare the cartographic SHG maps acquired experimentally to that of the FEM based numerical simulations.[11] The approach used here is to acquire the SHG intensity distribution over the entire nanoprism by simultaneously exciting and collecting the signal from the same positions. In other words, the SHG map does not correspond to a single plasmon mode rather it is a result of different plasmon modes excited as a function of position over the nanoprism. The simulation was therefore developed to account for the exact experimental configuration as briefly described in section 3). Figure 1 shows nanoprisms of size 707nm that was investigated. Chemically

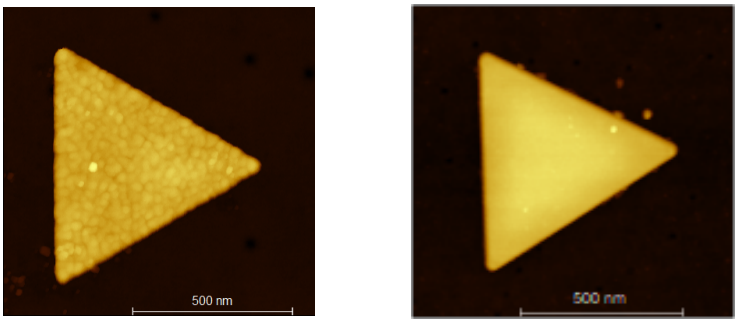

(a) (b)

Figure 1: 1a is an AFM image of a Gold nanoprism fabricated using E-beam lithography and 1b is an AFM image of a chemically synthesized Gold nanoprism

synthesized nanoprisms and lithographic nanoprisms of the same size were studied. The protocol used for the fabrication of these two nanoprisms were presented in the section 4. Figure 2 represents an experimental SHG map on the left acquired on chemically synthesized prisms which are then compared to the simulated individual nonlinear contributions as described in equations (5) presented on the right hand side. As the simulation does not take into account the transmission loss through various optical elements, the transmission efficiency of microscope objective and detection efficiency of the photon counting modules, the calculated signal counts represented in the simulated maps are normalized with the highest experimentally obtained intensity counts. Additionally, the red arrow in figure 2 represents polarization of the excitation field normal to the horizontal axis of the prism while blue arrow represents polarization of the detected photons that are normal and parallel to the same axis. In figure 2 one can note that the experimental SHG maps does not change with the change in detection polarization indicated by the blue arrows and there is only a single prominent lobe. In comparison with the simulations, the bulk contribution can be immediately ruled out as the intensity distribution itself is different from what is observed in the experimental map. Whereas, the discrimination between $\chi_{s\parallel\parallel\perp}$ and $\chi_{s\perp\perp\perp}$ is more ambiguous. However, noting that the intensity counts of the bulk contribution is dominant, it is evident that there is an apparent contradiction in our interpretation of the comparison made between the SHG maps. To explain this inconsistency, recall that the chemically synthesized nanoprisms are monocrystalline in nature, i.e they are essentially made up of single crystals arranged on top of each other thereby producing a low surface rugosity as it can be seen in the AFM image. In addition to it, recall that the $\chi_{s\parallel\parallel\perp}$ component represents parallel surface contribution generated by electric field components parallel and perpendicular to the surface. This contribution therefore arises from the parallel surface currents. Putting together these two points, rough surfaces displaying irregularities on the surface in the form of pits and bumps could affect the parallel current flow. The rough features could

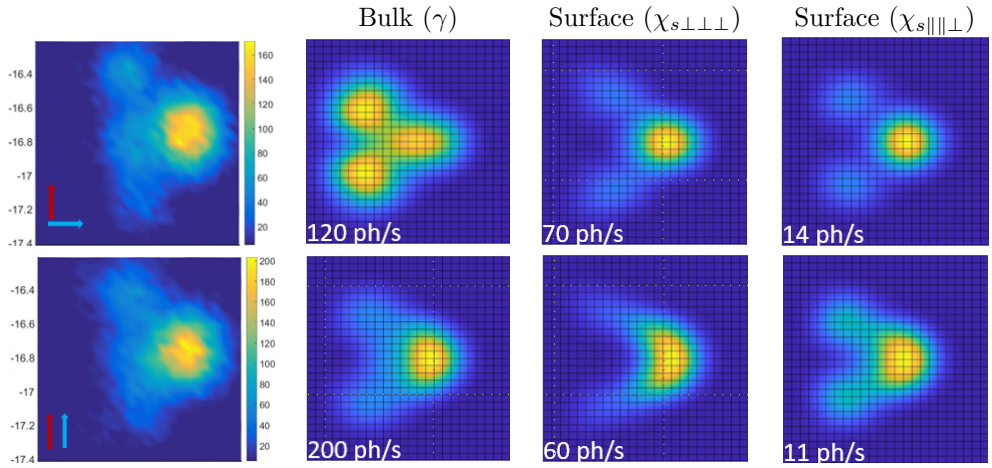

Figure 2: Represented on the left are maps obtained on crystalline prisms. On the right side are the simulations corresponding to the three individual nonlinear components. The red arrow represents polarization of the excitation field and blue arrow represents the polarization of the detected photons with respect to the horizontal axis of the prism in the x-y plane. The excitation wavelength is set at 880nm.

therefore scatter the electrons thereby affecting the parallel current represented by $\chi_{s\parallel\parallel\perp}$ component[12]. This could be taken into account through the weight given by the non-dimensional Rudnick-Stern parameter 'b' in $\chi_{s\parallel\parallel\perp}$ as shown in (5). According to the literature, b varies from 0.1 to 1 where the highest value represents a smooth perfectly reflecting boundary and the lowest value correspondingly represents a rougher surface.

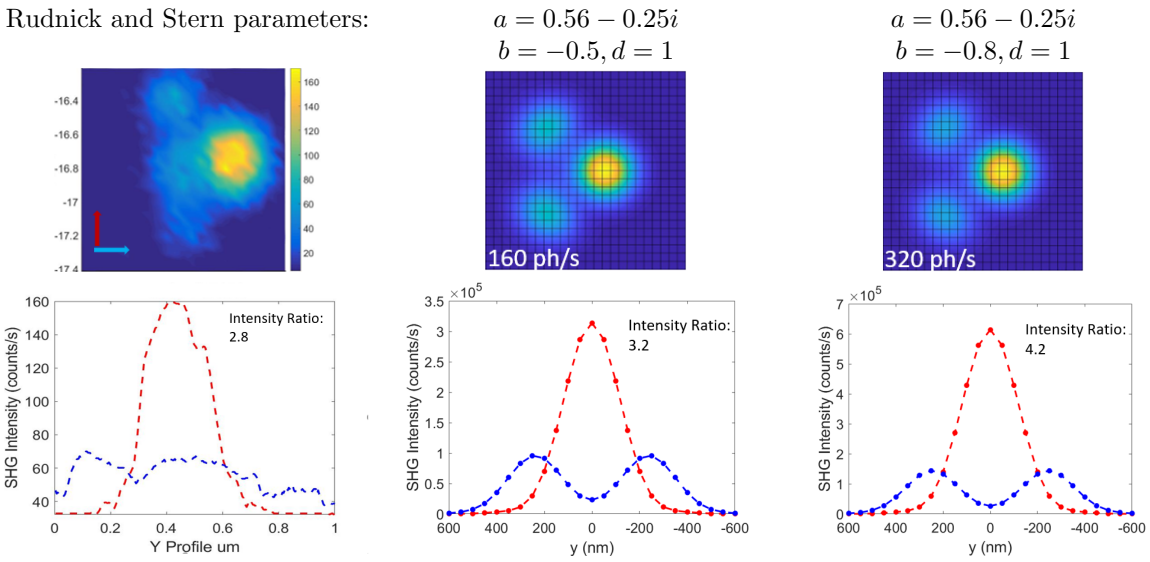

Figure 3: The simulations on right side represents a coherent sum of all the nonlinear contributions and the 'b' parameter corresponding to $\chi_{s\parallel\parallel\perp}$ is then varied. The intensity profile shows the ratio between the high intensity lobe and low intensity lobes.

Taking this into account, figure 3 shows a coherent sum of the three nonlinear components by varying the 'b' parameter. Here, it can be seen that the two symmetric lobes diminishes in intensity with b. In the experimental map, one can note the absence of a distinct three lobe pattern lobe which could be due to the characteristic nature of chemically synthesized prism. Regardless, the intensity ratio of the experimental

map on the left gives a value of 2.8. This ratio is closer to those given for $b = 0.5$ in the simulated maps. According to the literature,[4] $b = 0.5$ corresponds to a flat surface but which diffusely scatters electrons. Increasing the b further close to unity, one can see that contribution from parallel surface component augments the intensity of the bright lobe whereas the two side lobes diminishes in intensity. Therefore, from the intensity ratio, it is evident that the value of b that fits closest to the experimental data is b=-0.5.
To decouple the effect of roughness from the flatness of a surface, prisms of the same size as crystalline prisms were fabricated by E-beam lithography. As the nucleation and subsequent layer growth of deposited Gold atoms/molecules in electron gun evaporation does not yield a lattice like structure similar to a crystalline growth, the surface is therefore expected to exhibit significant roughness with increasing thickness. In figure 4 SHG maps obtained with lithographed prisms of varying thickness are compared with crystalline prisms for the same excitation wavelength and polarization shown in the previous figures as well as simulated SHG maps for the larger thickness. As it can be seen, the overall intensity distribution is similar across the three prisms. Additionally, the prism with a larger thickness displays a distinct and comparatively more intense three lobe response which is in agreement with the result obtained from the simulations. This agreement also indicates that the effect of roughness on the response is absent or negligible zince the simulation does not take into account the surface rugosity. One explanation put forth is that, the overall shape or the long range order of the surface of lithograph prism is flat but that contains horizontal features primarily determined by the grain size of Gold due to the process of electron gun deposition. From the point of view of electron scattering, the horizontal distance of a surface feature must be on the order of $\frac{v_f}{\omega}$ to affect the parallel surface current[4] . To put into perspective, for Gold given a wavelength of 1000nm, the value corresponds to 5Å-10Å. While the resolution at the angstrom level is inaccessible via AFM, one can note that the grain size of Gold via evaporation is larger than few tens of nanometer which is measurable. Thus, essentially one could argue that the horizontal feature distance is too big to observe the effect from electron scattering and consequently the surface roughness. This, therefore, is in agreement with the conclusion arrived for crystalline prisms while noting that the effect of roughness is not significant in the case of lithographic nanoprisms as it was expected.

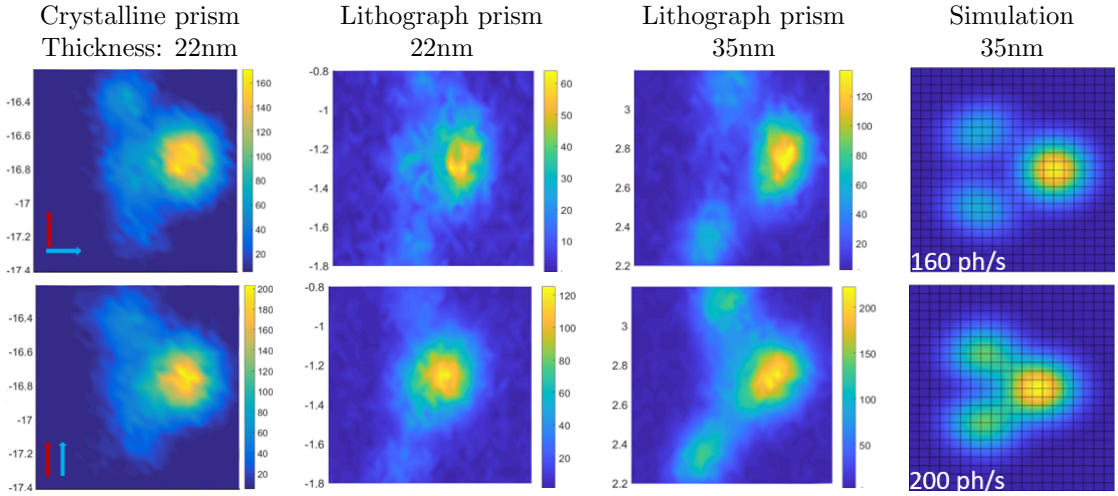

Figure 4: Simulated SHG maps and experimental maps corresponding to crystalline and lithographed gold nanoprisms of size 707nm Gold nanoprisms excited at 880nm with polarization perpendicular to the horizontal axis of nanoprisms in the x-y plane.

5.1 Conclusion

The generation of SHG in metals is attributed to three main contributions. Among the three, two contributions arise from the surface whereas the third comes from the bulk. Often in the literature, surface contribution, in particular, the one arising from the normal currents are attributed to have the dominant

role in SHG because of the breaking of centrosymmetry at the surface resulting in strong electric field gradient field discontinuity. In this report, we compare numerically simulated and experimentally acquired cartographic SHG response maps over a nanoprism to distinguish and determine the dominant SHG source contribution. The map is acquired by simultaneously exciting and collecting different positions on the nanoprism by scanning it under a high numerical aperture microscope objective. The resulting map obtained is therefore an SHG intensity distribution or the efficiency of harmonic response as a function of position over the nanoprism. The experimental configuration is quantitatively accounted for by means of numerical simulations based on finite element method whereby the substrate, high numerical aperture, reflection mode of the experiment are taken into account. In our experiment, chemically synthesized and lithographic nanoprisms of Gold of the same size were investigated. We demonstrate that the SHG source arising from the $\chi_{s\parallel\parallel\perp}$ surface contribution is the dominant contribution in the nanoprisms by comparing the response maps of the individual nonlinear SHG source contributions as well as their coherent response. Contrary to the literature, intensity from $\chi_{s\perp\perp\perp}$ is the weakest while that corresponding to the bulk γ has a non-trivial contribution and that from $\chi_{s\parallel\parallel\perp}$ remains dominant. Additionally, we verify the effect of roughness on the response by performing the same experiment on a nanoprism of larger thickness since the physical vapor deposition of Gold yields rougher layer with increasing thickness. The approach thus adopted in this investigation can also be extended to investigate the harmonic response from nanoantennas of any shapes or configurations of interest.

REFERENCES

[1] R. W. Boyd, Nonlinear Optics, Academic Press, Inc., 3rd ed. (2008)

[2] Paul G. Kwiat, Klaus Mattle, Harald Weinfurter and Anton Zeilinger, New High-Intensity Source of Polarization-Entangled Photon Pairs, Phys. Rev. Lett. 75, 4337 (1995)

[3] Jérémy Butet, Pierre-François Brevet and Olivier J. F. Martin, Optical Second Harmonic Generation in Plasmonic Nanostructures: From Fundamental Principles to Advanced Applications, ACS Nano, 9, 11, 10545–10562 (2015)

[4] J.Rudnick and E.A.Stern, Second-Harmonic Radiation from Metal Surfaces, Phys. Rev. B 4, 4274 (1971)

[5] F.Brown and R.E.Parks, Magnetic-dipole contribution to optical harmonics in silver, Phys. Rev. Lett. 16, 507 (1966)

[6] Fu Xiang Wang, Francisco J. Rodríguez, Willem M. Albers, Risto Ahorinta, J. E. Sipe and Martti Kauranen, Surface and bulk contributions to the second-order nonlinear optical response of a gold film, Phys. Rev. B 80, 233402 (2009)

[7] Sami Kujala, Brian K. Canfield and Martti Kauranen, Multipole Interference in the Second-Harmonic Optical Radiation from Gold Nanoparticles, Phys. Rev. Lett. 98, 167403 (2007)

[8] N. Feth, S. Linden, M. W. Klein, M. Decker, F. B. P. Niesler, Y. Zeng, W. Hoyer, J. Liu, S. W. Koch, J. V. Moloney and M. Wegener, Second-harmonic generation from complementary split-ring resonators, Optics Letters Vol. 33, Issue 17, pp. 1975-1977 (2008)

[9] Daniel Timbrell, Jian Wei Yo, Yuri S. Kivshar and Nicolae C. Panoiu, A comparative analysis of surface and bulk contributions to second-harmonic generation in centrosymmetric nanoparticles, Sci Rep 8, 3586 (2018)

[10] G. Bachelier, J. Butet, I. Russier-Antoine, C. Jonin, E. Benichou and P.-F. Brevet, Origin of optical second-harmonic generation in spherical gold nanoparticles: Local surface and nonlocal bulk contributions, Phys. Rev. B 82, 235403 (2010)

[11] Maëliss Ethis de Corny, Nicolas Chauvet, Guillaume Laurent, Mathieu Jeannin, Logi Olgeirsson, Aurélien Drezet, Serge Huant, Géraldine Dantelle, Gilles Nogues and Guillaume Bachelier, Wave-mixing origin and optimization in single and compact aluminum nanoantennas, ACS Photonics 2016, 3, 10, 1840–1846 (2016)

[12] J. E. Sipe, V. C. Y. So, M. Fukui, and G. I. Stegeman, Analysis of second-harmonic generation at metal surfaces, Phys. Rev. B 21, 4389 (1980)